49th AIAA Aerospace Sciences Meeting including the New Horizons Forum and Aerospace Exposition
4 - 7 January 2011, Orlando, Florida
AIAA 2011-732

Geometry Effects of Dielectric Barrier Discharge on a Flat Surface

Chin-Cheng Wang* and Subrata Roy§
Computational Plasma Dynamics Laboratory and Test Facility
Mechanical and Aerospace Engineering Department
University of Florida, Gainesville, FL 32611-6300

We present four different shapes of dielectric barrier discharge (DBD) actuators for the inducement of fluid flow. Three-dimensional plasma governing equations have been solved based on in-house MIG flow code. We numerically test these actuators in quiescent air. Numerical results show plasma force vectors as well as detailed flow behaviors such as velocity and vorticity. Novel designs of three-dimensional (triangular, serpentine, and square) actuators produce much strong flow mixing downstream of the actuator than traditional two-dimensional (linear) actuators. Specifically, square actuator has the best performance in flow mixing than others. Three-dimensional effects such as pinching or spreading the neighboring fluid become an important index to enhance the performance of the actuator.

Nomenclature

D_e	=	electron diffusion coefficient (cm^2/s)
D_i	=	ion diffusion coefficient (cm^2/s)
E	=	electric field (V/m)
e	=	elementary charge (C)
F	=	electric force density (N/m^3)
k_B	=	Boltzmann's constant (J/K)
m_i	=	ion mass (kg)
n_e	=	electron density (m^{-3})
n_i	=	ion density (m^{-3})
p	=	pressure (Torr)
q	=	charge density, (n_i-n_e) (m^{-3})
r	=	electron-ion recombination rate (cm^3/s)
T_e	=	electron temperature (K)
T_i	=	ion temperature (K)
t	=	time (s)
V_B	=	Bohm velocity (m/s)
V_e	=	electron velocity (m/s)
V_i	=	ion velocity (m/s)
V	=	fluid velocity (m/s)
α	=	Townsend coefficient (cm^{-1})
ε	=	dielectric constant (Farad/m)
ϕ	=	potential (V)
Γ_e	=	electron flux (m^{-2} s^{-1})
μ_e	=	electron mobility (cm^2/sV)
μ_i	=	ion mobility (cm^2/sV)
μ	=	fluid viscosity (kg/sm)
ρ	=	fluid density (kg/m^3)

* Research Scientist, Member AIAA, james614@ufl.edu
§ Associate Professor, Associate Fellow AIAA, roy@ufl.edu

I. Introduction

The plasma actuator is becoming a popular device for active flow control. The advantages of the plasma actuators are without moving parts and easy to compact on any location. Specially, the life will be much longer than mechanical reciprocal device such as synthetic jet actuator. Reported experimental and numerical data show that dielectric barrier discharge (DBD) actuators are useful in controlling the flow at low freestream velocities (~20m/s). One major impediment affecting the working speed is the inducement of a thin boundary layer which is limited by wall shear. So it is important to design actuators which can inject momentum into the boundary layer resulting in a much thicker layer.

Roth *et al*.[1] and Corke *et al*.[2] showed aerodynamic applications of standard DBD actuators on a flat plat at atmospheric pressures. The actuator produced a significant thrust by asymmetric spanwise electrode configurations. Subsequently, Shyy *et al*.[3] numerically test their experiments based on a phenomenological model of plasma body force. Many people directly use this plasma force model in computational fluid dynamics instead of solving plasma governing equations to reduce computational time. However, the phenomenological model is still lack of physical parameters. Other researchers[4-5] have developed reduced order plasma force model based on semi-empirical or physics based formulation. The model is considered not only the geometry effects but also plasma parameters. In reduced order model, the fidelity is much better than phenomenological model but it is still not enough to explain the physics of DBD actuator. First-principles analysis is a high-fidelity model to examine the physics of plasma actuator. Roy *et al*.[6-8] presented a well-established model to describe detailed densities of electrons, positive and negative charged and neutral species with Poisson's equation to obtain temporal and spatial profiles of voltage and densities. They demonstrated the model predictions for charge densities, electric field, and gas velocity distributions, and showed tend that mimic reported experimental data.

Experiments and simulations have shown that the momentum boundary layer is significantly influenced by plasma actuation in low speed regime. Gaitonde and Visbal *et al*.[9-10] investigated control of three-dimensional vortical structures using standard linear plasma actuators. They showed such actuator reduces or eliminates stall on the airfoil for a reference flow Reynolds number of 45,000. In their studies, the three-dimensional vortical structures were analyzed using essentially two-dimensional plasma effects. However, two-dimensional plasma characterization severely limits full exploration of the actuator design and its capability.

In our prior study[11], we presented the interaction of a serpentine actuator with a co-flow or counter-flow on a flat surface. We used reduced order models[4] to predict plasma forces as body forces and added them into Navier-Stokes equations. The results showed three-dimensional plasma effects extract momentum from an upstream flow injecting it into the bulk fluid through localized pinching and spreading effects. Such three-dimensional novel actuators produce much better flow mixing downstream of the actuator than standard two-dimensional (linear) actuator.

In the present study, we introduce novel triangular, serpentine and square actuators and compare them with traditional linear actuator. For high-fidelity force distribution of these designs, we employ physics based first-principles analysis to resolve the plasma force vectors distribution over a flat surface. The detailed numerical model is summarized in the section II. Section III describes the cases of numerical simulation for different shaped plasma actuators. Section IV presents the results of plasma force vectors, velocity streamtraces and vortical structures. Finally, conclusions are drawn in section V.

II. Numerical Model

Three-dimensional two species plasma governing equations as well as Navior-Stokes equations are solved in this study. The unsteady transport for ions and electrons is derived from the first-principles in the form of conservation of species continuity. The species momentum flux embedded in them using the drift-diffusion approximation under isothermal condition. Such approximation can predict general characteristics of plasma discharges.[12] The continuity equations for concentration of positive ion n_i and electron n_e together with Poisson equation for electric field vector $\mathbf{E}$ (E_x, E_y, E_z):

$$\nabla \cdot (\varepsilon \mathbf{E}) = -e(n_e - n_i) \tag{1}$$

$$\frac{\partial n_i}{\partial t} + \nabla \cdot \left(n_i \mathbf{V}_i \right) = \alpha \left| \Gamma_e \right| - r n_i n_e$$
$$\frac{\partial n_e}{\partial t} + \nabla \cdot \left(n_e \mathbf{V}_e \right) = \alpha \left| \Gamma_e \right| - r n_i n_e \tag{2}$$
$$\left| \Gamma_e \right| = \sqrt{(n_e V_e)_x^2 + (n_e V_e)_y^2 + (n_e V_e)_z^2}$$

where n_e and n_i are number densities of electron and ion respectively, $\mathbf{V}$ (V_x, V_y, V_z) is the species hydrodynamic velocity, $r \sim 2\times10^{-7}$ cm^3/s is the electron-ion recombination rate, ε is the dielectric constant, the elementary charge e is 1.6022×10^{-19} C, and subscript i and e are positive ion and electron, respectively. The discharge is maintained using a Townsend ionization scheme. The ionization rate is expressed as a function of electron flux $\left|\Gamma_e\right|$ and Townsend coefficient α:

$$\alpha = Ap \exp\left(-B/(\left|\mathbf{E}\right|/p)\right) \tag{3}$$

where A and B are preexponential and exponential constants, respectively, p is the gas pressure, and E is the electric field. The ionic and electronic fluxes in equation (2) are written as:

$$n_i \mathbf{V}_i = n_i \mu_i \mathbf{E} - D_i \nabla n_i$$
$$n_e \mathbf{V}_e = -n_e \mu_e \mathbf{E} - D_e \nabla n_e \tag{4}$$

Finally, we end up with the following equations:

$$\frac{\partial n_i}{\partial t} + \frac{\partial}{\partial x}\left\{ n_i \mu_i E_x - D_i \frac{\partial n_i}{\partial x} \right\} + \frac{\partial}{\partial y}\left\{ n_i \mu_i E_y - D_i \frac{\partial n_i}{\partial y} \right\} + \frac{\partial}{\partial z}\left\{ n_i \mu_i E_z - D_i \frac{\partial n_i}{\partial z} \right\} = \alpha \left| \Gamma_e \right| - r n_i n_e$$
$$\frac{\partial n_e}{\partial t} + \frac{\partial}{\partial x}\left\{ -n_e \mu_e E_x - D_e \frac{\partial n_e}{\partial x} \right\} + \frac{\partial}{\partial y}\left\{ -n_e \mu_e E_y - D_e \frac{\partial n_e}{\partial y} \right\} + \frac{\partial}{\partial z}\left\{ -n_e \mu_e E_z - D_e \frac{\partial n_e}{\partial z} \right\} = \alpha \left| \Gamma_e \right| - r n_i n_e \tag{5}$$

where $\mu_i = 1.45\times10^3 / p$ (cm^2/sV) is the ion mobility, $\mu_e = 4.4\times10^5 / p$ (cm^2/sV) is the electron mobility, D_i and D_e are the ion and electron diffusion coefficients calculated from the Einstein relation which is a function of ion and electron mobility as well as ion and electron temperature, i.e. $D_i = \mu_i T_i$ and $D_e = \mu_e T_e$. The electric field is given by $\mathbf{E} = -\nabla\varphi$, i.e., the gradient of electric potential φ. The system of equation (1) is normalized using the following normalization scheme: $\tau = t/t_0$, $z_i = x_i/d$, $N_e = n_e/n_0$, $N_i = n_i/n_0$, $u_e = V_e/V_B$, $u_i = V_i/V_B$, and $\phi = e\varphi/k_B T_e$ where k_B is Boltzmann's constant, $V_B = \sqrt{k_B T_e / m_i}$ is the Bohm velocity, reference length d which is usually a domain characteristic length in the geometry.

The numerical model for solving DBD plasma governing equations uses an efficient finite element algorithm for solving partial differential equations (PDE) approximately. The solution methodology anchored in the modular MIG flow code is based on the Galerkin Weak Statement (GWS) of the PDE which is derived from variational principles. An iterative sparse matrix solver called Generalized Minimal RESidual (GMRES) is utilized to solve the resultant stiff matrix. The fully implicit time stepping procedure along with the Newton-Raphson scheme is used for dealing with this nonlinear problem. The solution is assumed to have converged when the L_2 norms of all the normalized solution variables and residuals are below a chosen convergence criterion of 10^{-3}.

The established three-dimensional fluid model is solved by a commercial CFD package, ANSYS FLUENT 12. We interpolate the time-averaged electric force density as a source term in the momentum equations using user defined functions (UDF). A second-order upwind discretization method is used. Convergence is determined when the residual among the continuity and momentum equations are less than 10^{-3}. The density of computational mesh of 500,000 cells is applied to fluid domain. For an incompressible Newtonian fluid, the Navier-Stokes equation is:

$$\nabla \cdot \mathbf{V} = 0$$
$$\rho \frac{D\mathbf{V}}{Dt} = \rho f - \nabla p + \mu \nabla^2 \mathbf{V} \tag{6}$$

where $\mathbf{V}$ (V_x, V_y, V_z) is the fluid velocity, $\rho f = \mathbf{F} = eq\mathbf{E}$ is the body force density, and μ is the viscosity of fluid.

III. Problem Description

We numerically test four different shapes of plasma actuators at the center of a quiescent domain with dimensions of 0.2x0.2x0.1m. Figure 1 describes schematics of a fluid computational domain and a serpentine plasma actuator on a flat surface. The plasma actuators are assumed to be flushed mounted at the center of a quiescent domain with dimensions (-0.1:0.1×-0.1:0.1×0:0.1) m. For the flow boundary conditions, the right side of the domain (y = 0.1 m) is considered to be the inlet, while the top (z = 0.1 m) and left (y = -0.1 m) sides are outflow boundaries. The gauge pressure at the outlet boundaries is maintained at 0 Pa. Symmetry is considered on the domain's side walls (x = ±0.1 m), while no slip is enforced on the lower boundary (z = 0.0 m). The computational mesh of plasma domain consists of 89x49x41 nodes. We first calculate plasma force distribution from plasma domain and then interpolate these data into fluid domain to get the inducement of vortical structures. The thickness of the dielectric material and electrodes are neglected in the flow simulations. Air is considered to be the working fluid.

The plasma actuator consists of two electrodes and separates by a dielectric material. The aim of this study is to design actuators which can turbulize the flow effectively. Upon applying a sufficient electric field to the exposed electrode to induce an electrical breakdown, an electro-hydrodynamic (EHD) body force is generated along the electrode. This electric force interacts with bulk fluid and induces vortices locally and downstream of the actuator. Here, we present new designs of three-dimensional DBD actuators which are triangular, serpentine and square actuators shown in figure 2. The traditional two-dimensional linear actuator is considered as a baseline case. The merit of three-dimensional plasma actuators are able to induce strong vortices locally and downstream of the actuator. The details of vorticity generation using plasma actuators will be explained in the result section.

IV. Results and Discussion

The four different actuator configurations are simulated in quiescent air. We assume a time averaged electric plasma force as a body source term in the flow domain. Figure 3 shows force vectors overlaid on potential contour in the xy-plane. We can see the force vectors are acting from the powered electrode (red) to the grounded electrode (blue). Based on the distribution of force vectors, we can see the force vectors always perpendicular to the edges of electrodes. From top view of the linear actuator, the force vectors are even and perpendicular to the edges of electrodes. Also, for other shaped plasma actuators, the force vectors follow their shapes of electrodes. That's why the force vectors of linear actuator only act in one direction (y-direction). Based on the numerical results, the magnitude of electric force vectors for triangular, serpentine and square actuators is locally much larger than the linear case. This is a result of the local concentration electric fields as a result of the electrode geometry. Specially, serpentine and square designs have much stronger pinching effect than other designs. The influence of pinching effect is to change the flow direction from surface parallel to surface normal. Therefore one can say that the shape of the electrodes dominates the distribution of the electric force vectors.

Figure 4 shows electric force vectors overlaid on force (F_y) contours in the yz-plane (x = 0) at center of the actuator. The highest force level is colored by blue while the smallest one is colored by red. The force vectors are acting from powered electrode to grounded one in a projectile motion. For linear actuator, we can see the force vectors are nominally two dimensional primarily changing in the streamwise direction (y-direction). That is why there is no need to conduct a three-dimensional simulation to analyze a traditional two-dimensional linear actuator. However, it is important to conduct a three-dimensional simulation for our new designs (i.e. triangular, serpentine and square actuators). The force resulting from the linear configuration is predominately parallel to the surface, while the other actuators produce a force that follows more of a projectile profile which stems from the powered electrode to the grounded electrode. From the figure 4, it is clear to see the force distributions are purely three-dimensional for the actuators such as triangular, serpentine, and square designs.

Figure 5 shows streamtraces overlaid on streamwise velocity (V_y) contour above a flat surface (z = 0.002 m). We can see the fluid is attracted from upstream (top side), and is accelerated in the vicinity of plasma region, and then is pushed downstream of the actuator (bottom side). Due to end effects of electrodes for all cases, we can see significant changes in streamwise velocity on the sides of the actuators. In xy-plane, the pinching and spreading effects can be easily observed via streamtraces. For the downstream of serpentine and square actuators, the pinching region is where the jets of fluid merge. Based on the magnitude of streamwise velocity (y-velocity), serpentine and

square actuators have much higher y-velocity (blue) in the vicinity of the pinching region. The space between two pinching regions is a spreading area of fluid. Both pinching and spreading effects are pushing the fluid forward in streamwise direction. In addition, the pinching effect changes flow momentum to the vertical direction while the spreading effect keeps the flow attached to the surface. In contrast, for the linear actuator, the downstream streamwise velocity contour is even distributed without any changes caused by upward and downward motions.

Figure 6 shows streamtraces overlaid on spanwise velocity contour (V_x) at xz-plane ($y = 0$). We can see the flow is attracted from top side and is pinched at the center of the domain. For the linear actuator, the plasma force vectors are acting in one direction, so streamwise velocity (y-velocity) dominates the vicinity of plasma region. That is why there is no streamtraces close to surface in xy-plane. For the three-dimensional (triangular, serpentine and square) actuators, the pinching effect can be observed based on the spanwise velocity (x-velocity) at x=0. For the triangular actuator, the pinching force is not enough to make a rapid momentum change. Note that serpentine and square actuators induce much higher spanwise velocity on both left and right sides, and then change flow direction from surface parallel (x-direction) to surface normal (z-direction). Specially, for the square actuator, it injects a strong vertical momentum into the bulk region and results in a counter-rotating vortex pair.

Figure 7 shows streamtraces overlaid on vertical velocity contour (V_z) for the yz-plane ($x = 0$). We can see the flow is attracted from the right side and is pinched at center (y = 0) of the domain, and then moves forward downstream of the actuators. These arrow headed lines also show that the flow is rapidly moving downward and upward downstream after the pinching region. For the linear actuator, there is no pinching effect, so the plasma induced surface jet is issued in an angle of 8 degrees. For the triangular actuator, there is a little pinching effect which causes the momentum transfer into vertical direction. We can see a jet issuing angle of 12 degrees which is higher than the linear actuator. For the serpentine and square designs, the pinching effects result in a large normal velocity way from the wall. Here, the plasma jet issuing angle is 33 degrees for square actuators. Based on jet angles of the plasma actuators, we can say that three-dimensional square actuator has much stronger pinching effects than other designs.

Figure 8 shows instantaneous streamwise (y) vortical structures that are induced by four different actuator shapes after 16 milliseconds of operation. In figure 8, the iso-surfaces colored by red and blue depict y-vorticity at ±1000 1/sec. The y-vorticity (ω_y, i.e. streamwise vorticity) is defined as curl of fluid velocity determined by the derivative in the spanwise ($\partial u/\partial z$) and vertical ($\partial w/\partial x$) directions. For the two-dimensional linear actuator (baseline case), it only has velocity changes in streamwise (y) and vertical (z) directions. For the linear actuator (baseline case), there is only one $\partial w/\partial x$ term that dominates the flow of fluid downstream of the actuator. The instantaneous y-vorticity contour of blue and red color means the spin directions on both clockwise and counter-clockwise. The spin direction is caused by the rapid changes in vertical velocity because the surface plasma actuator attracts fluid from top (i.e. z-direction) boundary and changes flow direction from downward (surface normal) to upward and then forward downstream (surface parallel). The size of y-vorticity for the linear (two-dimensional) actuator is much smaller than three-dimensional ones because of less effect of pinching and spreading. For three-dimensional (triangular, serpentine and square) actuators, both $\partial u/\partial z$ and $\partial w/\partial x$ terms are important for vorticity generation. Specially, the term of $\partial u/\partial z$ dominates flow field for serpentine and square actuators. The term of $\partial u/\partial z$ can be used to represent the rapid changes in spanwise velocity which causes pinching and spreading effects. The pinching effect changes the flow direction from surface normal to surface parallel while the spreading effect pushes the fluid outward and forward downstream of the actuator. When both effects happen at same the time, they make fluid rapid rotational and translational motions in all three directions. Notably serpentine and square actuators are capable of inducing mixing much further downstream (in the y-direction) than the baseline two-dimensional linear actuator. For the square actuator, it has much bigger size of y-vorticity than other designs. So it will be very useful to induce a strong flow mixing as a vortex generating device. Due to the ends effects of the actuators, a stronger vorticity generation is presented near the sides of the domain. Otherwise, one will not be able to see much streamwise vorticity generation for the linear actuator.

V. Conclusion

The plasma governing equations as well as Navier-Stokes equations were solved with our in-house MIG flow code and commercial software ANSYS FLUENT. The configurations of four different electrode shapes are investigated in the present study. The results show traditional two-dimensional (linear) actuator is less effective at introducing streamwise vortical structures as compared to the other designs. It was numerically predicted that the serpentine and square designs are capable of producing significant three-dimensional effects which leads to enhance mixing of the surrounding fluid. Specially, square actuator shows much better mixing at downstream of the actuator. Realistic experimentation confirming these predictions is also repeated by R. Durscher and S. Roy[13]. For high-fidelity plasma simulation, the current three-dimensional modeling capability of plasma actuators is being enhanced with vibrational non-equilibrium air chemistry.

Acknowledgments

This work was partially supported by the AFOSR Grant FA9550-09-1-0372 and monitored by Dr. Douglas Smith.

References

[1]Roth, J. R., Sherman, D. M. and Wilkinson, S. P., 1998, "Boundary layer flow control with a one atmosphere uniform glow discharge surface plasma", 36th AIAA Aerospace Sciences Meeting and Exhibit, AIAA-98-0328.

[2]Corke, T. C., Jumper, E. J., Post, M. L., Orlov, D. and McLaughlin, T. E., 2002, "Application of weakly-ionized plasmas as wing flow-control devices", 40th AIAA Aerospace Sciences Meeting and Exhibit, AIAA-2002-350.

[3]Shyy, W., Jayaraman, B. and Andersson, A., 2002, "Modeling of glow discharge-induced fluid dynamics", *J. Appl. Phys.* 92(11), 6434-6443.

[4]Singh, K. P. and Roy, S., 2008, "Force approximation for a plasma actuator operating in atmospheric air", *J. Appl. Phys.* 103, 013305.

[5]Orlov, D. M. and Corke, T. C., 2005, "Numerical simulation of aerodynamic plasma actuator effects", 43rd AIAA Aerospace Sciences Meeting and Exhibit, AIAA-2005-1083.

[6]Roy, S., 2005, "Flow actuation using radio frequency in partially ionized collisional plasmas", *Appl. Phys. Lett*. 86, 101502.

[7]Kumar, H. and Roy, S., 2005, "Multidimensional hydrodynamic plasma-wall model for collisional plasma discharges with and without magnetic field effects", *Phys. Plasmas* 12, 093508.

[8]Singh, K. P., Roy, S. and Gaintonde, D. V., 2006, "Modeling of dielectric barrier discharge plasma actuator with atmospheric air chemistry", 37th AIAA Plasmadynamics and Lasers Conference, AIAA-2006-3381.

[9]Gaintonde, D. V.,Visbal, M. R. and Roy, S., 2006, "Three-dimensional plasma-based stall control simulations with coupled first-principles approached", ASME Joint US – European Engineering Summer Meeting, FEDSM2006-98553.

[10]Visbal, M. R. and Gaintonde, D. V., 2006, "Control of vortical flows using plasma actuators", 44th AIAA Aerospace Sciences Meeting and Exhibit, AIAA-2006-505.

[11]Roy, S. and Wang, C.-C, 2009, "Bulk fluid modification with horseshoe and serpentine plasma actuator", *J. Phys. D: Appl. Phys.* 42, 032004.

[12]Surzhikov, S. T. and Shang, J. S., 2004, "Two-component plasma model for two-dimensional glow discharge in magnetic field", *J. Comput. Phys*. 199, 437-464.

[13]Durscher, R. and Roy, S., "Induced Flow from Serpentine Plasma Actuators Acting in Quiescent Air", 49th AIAA Aerospace Sciences Meeting including the New Horizons Forum and Aerospace Exposition, AIAA-2011.

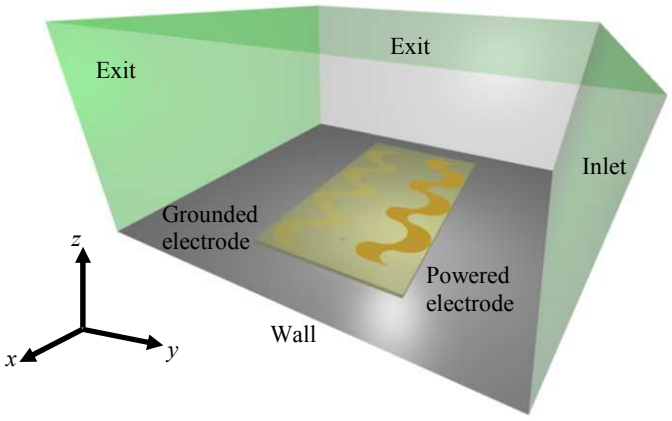

Figure 1. Schematics of computational domain and serpentine actuator.

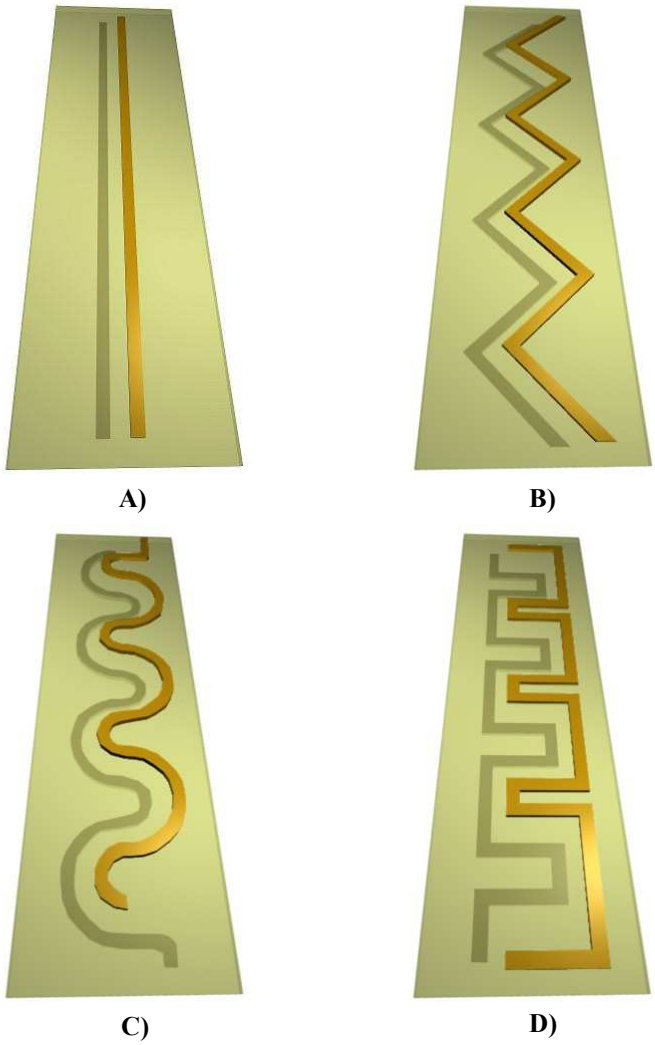

Figure 2. Schematics of plasma actuator for A) linear, B) triangular, C) serpentine, and D) square designs.

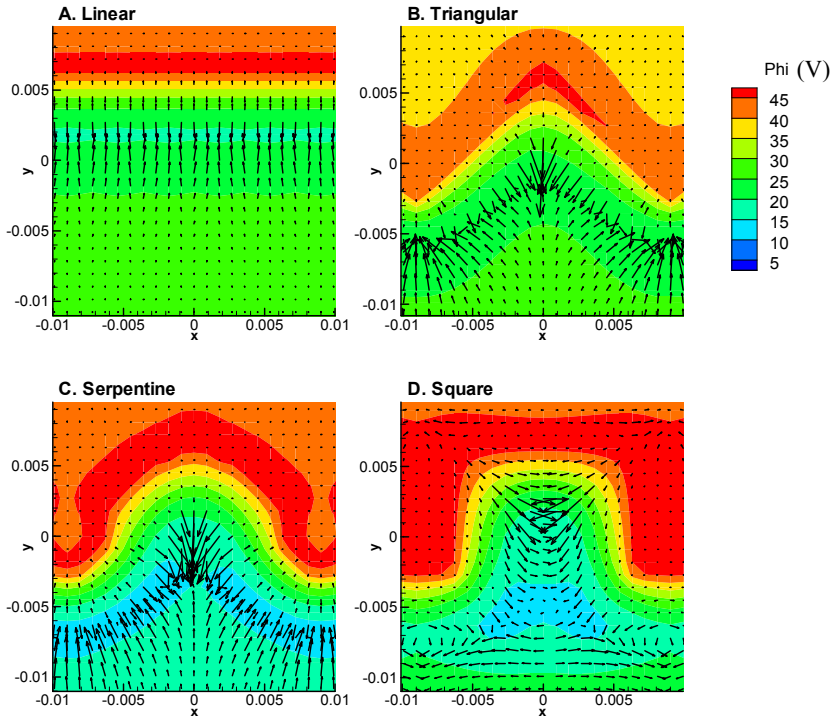

Figure 3. Plasma force vectors overlaid on potential contour (Phi) on the *xy*-plane for four different designs.

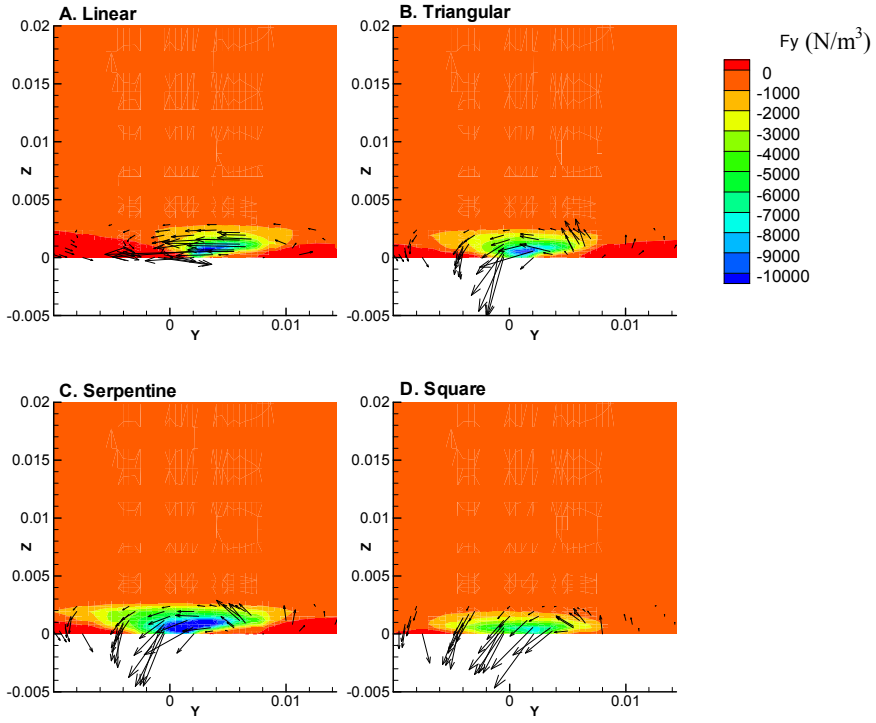

Figure 4. Plasma force vectors overlaid on y-force contour (F_y) on the *yz*-plane for four different designs.

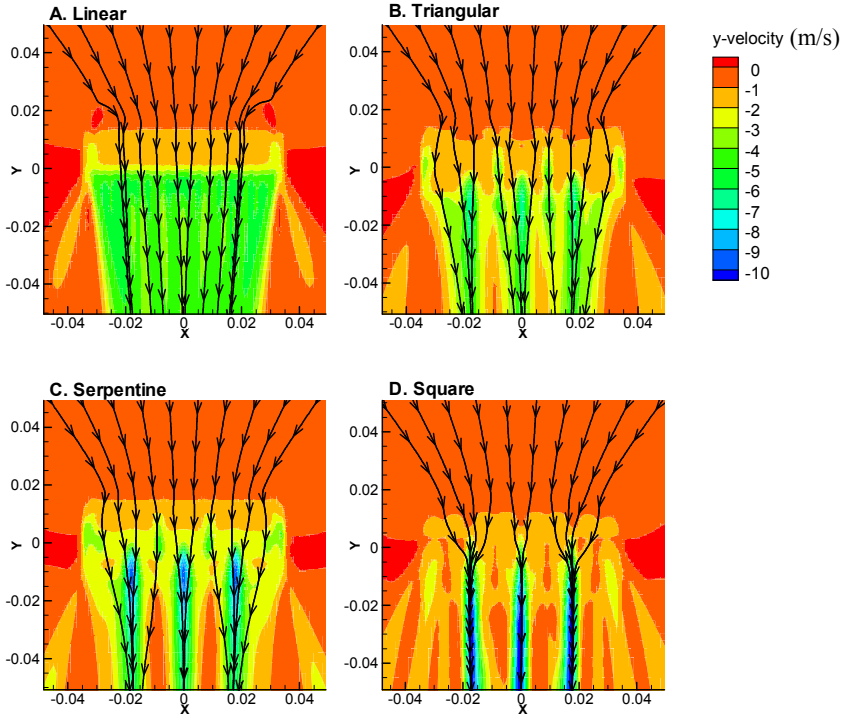

Figure 5. Streamtraces overlaid on *y*-velocity contour (V_y) on the *xy*-plane for four different designs.

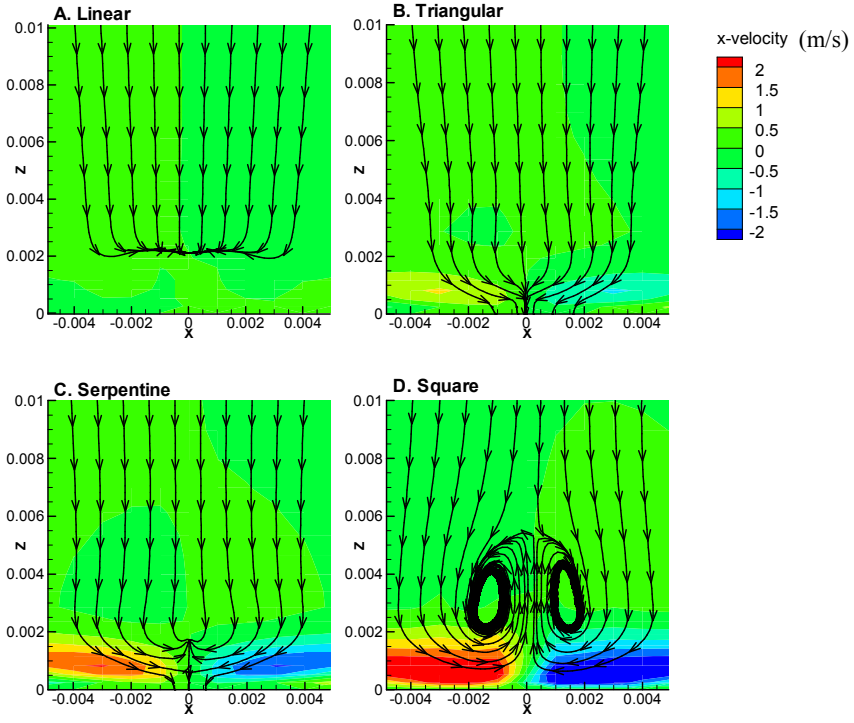

Figure 6. Streamtraces overlaid on x-velocity contour (V_x) on the *xz*-plane for four different designs.

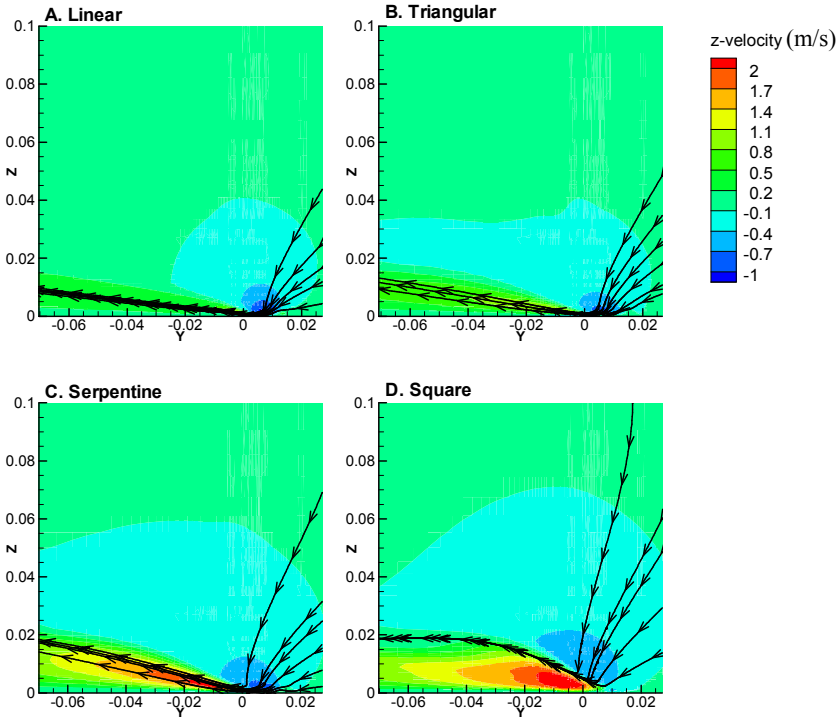

Figure 7. Streamtraces overlaid on *z*-velocity contour (V_z) on the *yz*-plane for four different designs.

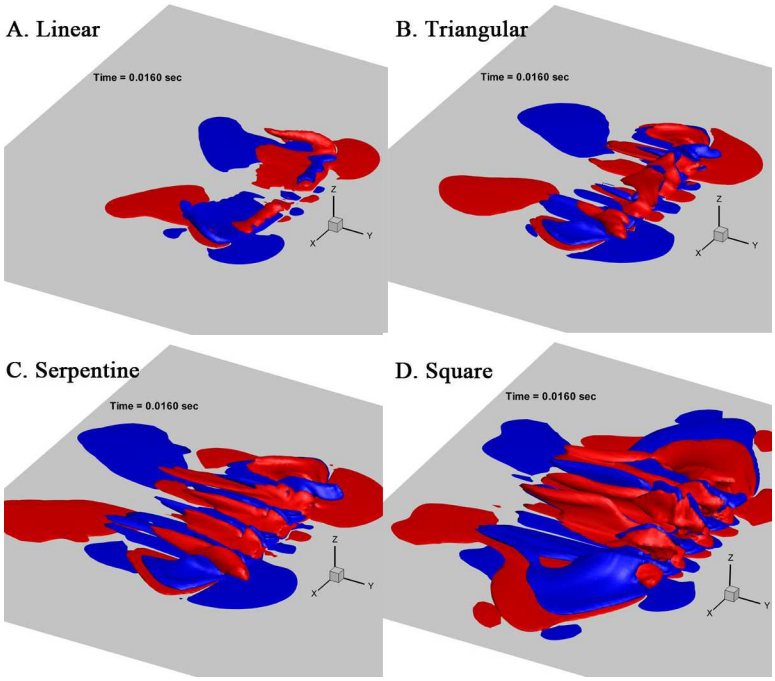

Figure 8. Three-dimensional dynamics of *y*-vorticities (+1000; -1000 1/s) for four different designs.